


BRIEF DEFINITIVE REPORT

A homozygous SFTPA1 mutation drives necroptosis of type II alveolar epithelial cells in patients with idiopathic pulmonary fibrosis

Akio Takezaki^{1,2}, Shin-ichi Tsukumo^{1,3}, Yasuhiro Setoguchi^{4,5}, Julie G. Ledford⁶, Hisatsugu Goto², Kazuyoshi Hosomichi⁷, Hisanori Uehara⁸, Yasuhiko Nishioka^{2,9}, and Koji Yasutomo^{1,3,9} 

Idiopathic pulmonary fibrosis (IPF) is a fatal disease characterized by scattered fibrotic lesions in the lungs. The pathogenesis and genetic basis of IPF remain poorly understood. Here, we show that a homozygous missense mutation in *SFTPA1* caused IPF in a consanguineous Japanese family. The mutation in *SFTPA1* disturbed the secretion of SFTPA1 protein. *Sftpa1* knock-in (*Sftpa1-KI*) mice that harbored the same mutation as patients spontaneously developed pulmonary fibrosis that was accelerated by influenza virus infection. *Sftpa1-KI* mice showed increased necroptosis of alveolar epithelial type II (AELI) cells with phosphorylation of IRE1 α leading to JNK-mediated up-regulation of Ripk3. The inhibition of JNK ameliorated pulmonary fibrosis in *Sftpa1-KI* mice, and overexpression of Ripk3 in *Sftpa1-KI* mice treated with a JNK inhibitor worsened pulmonary fibrosis. These findings provide new insight into the mechanisms of IPF in which a mutation in *SFTPA1* promotes necroptosis of AELI cells through JNK-mediated up-regulation of Ripk3, highlighting the necroptosis pathway as a therapeutic target for IPF.

Introduction

Idiopathic pulmonary fibrosis (IPF) is characterized by scattered fibrotic lesions in the lungs and has a median survival time of <3 yr (Raghu, 2011; Steele and Schwartz, 2013; Ahluwalia et al., 2014). The pathogenesis of IPF is poorly understood, and no effective approaches are available to reverse the development of pulmonary fibrosis. Previous papers have proposed that IPF is caused by repeated injury to alveolar epithelial cells, resulting in excessive and sustained fibroblast activation and subsequent accumulation of matrix-producing myofibroblasts (Noble et al., 2012). The environmental and genetic factors underlying sporadic IPF are unknown, though cases of familial IPF have been linked to mutations in telomerase (Armanios, 2013; Steele and Schwartz, 2013; Putman et al., 2014). A genome-wide linkage analysis revealed that variants in the promoter region of *MUC5B* were strongly associated with IPF (Seibold et al., 2011). A rare heterozygous missense mutation in *SFTPA2*, which encodes surfactant protein A (SP-A) 2, was also reported; SFTPA2 proteins carrying the mutation were retained in the ER and

therefore not secreted (Wang et al., 2009). SFTPA2 forms a complex with SFTPA1, which is secreted into the alveolar space as SP-A (Maitra et al., 2010). A heterozygous missense mutation in *SFTPA1* was also found in IPF patients (Nathan et al., 2016). However, it remains unclear how the mutations in *SFTPA1* or *SFTPA2* are associated with the pathogenesis of IPF.

Necroptosis is thought to be a pro-inflammatory type of cell death that releases intracellular contents that stimulate immune cells (Galluzzi and Kroemer, 2008; Pasparakis and Vandenabeele, 2015; Silke et al., 2015). The necroptosis machinery comprises receptor interacting serine/threonine kinase 3 (RIPK3) and pseudokinase mixed lineage kinase-like (MLKL). RIPK3 is activated through TNF receptor families, TLR3, TLR4, or DNA sensor (He et al., 2011; Li et al., 2012; Vanden Berghe et al., 2014). Autophosphorylated RIPK3 phosphorylates MLKL, which drives its oligomerization and translocation to membranes (Sun et al., 2012; Rickard et al., 2014). Although necroptosis is known to contribute to several

¹Department of Immunology & Parasitology, Graduate School of Medicine, Tokushima University, Tokushima, Japan; ²Department of Respiratory Medicine, Graduate School of Medicine, Tokushima University, Tokushima, Japan; ³Department of Interdisciplinary Researches for Medicine and Photonics, Institute of Post-LED Photonics, Tokushima University, Tokushima, Japan; ⁴Department of Respiratory Medicine, Graduate School of Medicine, Tokyo Medical University, Tokyo, Japan; ⁵Department of Respiratory Medicine, Graduate School of Medical and Dental Sciences, Tokyo Medical and Dental University, Tokyo, Japan; ⁶Department of Cellular and Molecular Medicine, University of Arizona, Tucson, AZ; ⁷Department of Bioinformatics and Genomics, Graduate School of Advanced Preventive Medical Sciences, Kanazawa University, Ishikawa, Japan; ⁸Division of Pathology, Tokushima University Hospital, Tokushima, Japan; ⁹The Research Cluster Program on Immunological Diseases, Tokushima University, Tokushima, Japan.

Correspondence to Koji Yasutomo: yasutomo@tokushima-u.ac.jp.

© 2019 Takezaki et al. This article is distributed under the terms of an Attribution–Noncommercial–Share Alike–No Mirror Sites license for the first six months after the publication date (see <http://www.rupress.org/terms/>). After six months it is available under a Creative Commons License (Attribution–Noncommercial–Share Alike 4.0 International license, as described at <https://creativecommons.org/licenses/by-nc-sa/4.0/>).

types of pathological injury and inflammation (Moriwaki and Chan, 2013; Pasparakis and Vandenabeele, 2015; Silke et al., 2015), the contribution of necroptosis to human diseases is unclear.

Recent advances in exome resequencing have helped identify various disease-causing genes in inherited diseases even in single family or two families (Kitamura et al., 2011, 2014). Here, we describe the identification of a homozygous missense mutation in *SFTPA1* in patients of a consanguineous Japanese family. The homozygous missense mutation led to the failure of SP-A secretion. Mice that harbored the same mutation in *Sftpa1* (*Sftpa1* knock-in [*Sftpa1*-KI] mice) developed an IPF-like disease that was accelerated by influenza virus infection, leading to increased death of alveolar epithelial type II (AEII) cells. The deletion of *Ripk3* or *Mkl1* from *Sftpa1*-KI mice ameliorated the pulmonary fibrosis, indicating that necroptosis is involved in cell death. We also found that increased phosphorylation of IRE1 α (a component of ER stress responses) led to phosphorylation of JNK in AEII cells in *Sftpa1*-KI mice, which up-regulated *Ripk3*. The inhibition of IRE1 α or JNK ameliorated pulmonary fibrosis in *Sftpa1*-KI mice. In addition, overexpression of *Ripk3* in JNK inhibitor-treated *Sftpa1*-KI mice exacerbated pulmonary fibrosis. These findings provide new insights into the mechanisms of IPF by suggesting that the enhancement of necroptosis is crucial for pulmonary fibrosis. We highlight the necroptosis pathway as a future therapeutic target for IPF.

Results and discussion

Patient history and genetic analysis

In a single Japanese family with consanguineous marriage, two of the sons were diagnosed with IPF at the ages of 24 and 27 yr and died at 32 and 34 yr, respectively (Fig. S1 a; Yoshioka et al., 2004). The youngest brother also began to develop dyspnea at the age of 40 yr. These patients were diagnosed using the criteria outlined in the official American Thoracic Society/Euroean Respiratory Society/Japanese Respiratory Society/Latin American Thoracic Association clinical practice guidelines (Raghu et al., 2018). Given the consanguinity of the family, an autosomal-recessive disease-causing variant was suspected. The parents of the patients do not show any clinical signs of pulmonary fibrosis, although they were not evaluated by computed tomography analysis. We performed homozygosity mapping, linkage analysis, and exome resequencing to find 15 shared rare variants between the two older brothers. Among those 15 rare variants, we found a homozygous missense mutation in *SFTPA1* (T622C) located in the homozygous region shared by the two older brothers (Fig. S1 b). This variant is not present in several human genetic variation databases, including the 1000 Genomes Project and the Exome Aggregation Consortium. The variant showed co-segregation with the disease under the assumption of autosomal-recessive inheritance, with both parents being heterozygous for the detected variant. This mutation changed the amino acid at position 208 from tyrosine to histidine (Fig. S1 b) and is located in the carbohydrate recognition domain (Fig. S1 b).

A mutation in *SFTPA1* disrupts the secretion of *SFTPA1*

To evaluate the effect of this *SFTPA1* mutation on its expression, secretion of *SFTPA1* protein, or complex formation with *SFTPA2*, WT Flag tagged-*SFTPA1* (Fig. S1 c), or *SFTPA2* (Fig. S1 d), was co-transfected with myc-tagged WT or mutant *SFTPA1*, and their association in the cell pellet or supernatant was evaluated by immunoprecipitation with an anti-Flag antibody and blotting with an anti-myc antibody (Fig. S1, c and d). The WT *SFTPA1* protein complexed with *SFTPA1* (Fig. S1 c) or *SFTPA2* (Fig. S1 d) in the cell pellets and supernatants as previously reported (Maitra et al., 2010). The mutant *SFTPA1* protein complexed with *SFTPA2* in cell pellets. However, mutant *SFTPA1*-WT *SFTPA1* or mutant *SFTPA1*-WT *SFTPA2* complexes were scarcely detected in the supernatants (Fig. S1, c and d). These data suggest that the mutation in *SFTPA1* disrupts the secretion of *SFTPA1*.

Mice carrying the mutation in *SFTPA1* spontaneously developed pulmonary fibrosis

To determine if the *SFTPA1* mutation in this family contributed to IPF development, we created mice (*Sftpa1*-KI) that carried the same mutation in the mouse gene *Sftpa1* (Y208H; Fig. S2 a). The homologous recombination of the construct harboring the mutant *Sftpa1* was confirmed by Southern blotting (Fig. S2 a). Mice born with normal Mendelian frequency showed growth rates similar to WT and did not show any differences in the frequencies of immune cells, including T cells, B cells, macrophages, and dendritic cells in the spleen and lymph nodes (data not shown).

We next evaluated the secretion of *Sftpa1* in *Sftpa1*-KI mice. The bronchoalveolar lavage (BAL) fluid from *Sftpa1*-KI mice did not contain *SFTPA1* (Fig. 1 a). In contrast, in WT mice, high production of *SFTPA1* was found in BAL fluid (Fig. 1 a). The lung tissue samples in *Sftpa1*-KI mice expressed equivalent levels of *SFTPA1* (Fig. 1 a). These findings were in line with the impaired secretion of mutant human *SFTPA1* in transfected A549 cells.

The *Sftpa1*-KI mice were healthy at ages 8–30 wk but began to die around 40 wk of age (Fig. 1 b). The lung sections of *Sftpa1*-KI mice showed increased cell infiltration and fibrotic regions at the age of 35 wk (Fig. 1 c). These pathological changes were not detected at 20 wk of age in *Sftpa1*-KI mice but were evident at 35 wk of age (Fig. 1 c). We evaluated type 1 collagen mRNA (*Colla1*; Fig. 1 d) and hydroxyproline (Fig. 1 e) at the ages of 10, 20, and 30 wk. We began to detect increased *Colla1* mRNA and hydroxyproline at the ages of 20 and 30 wk, respectively. The arterial PaO₂ levels of *Sftpa1*-KI mice at 10 and 20 wk of age were equivalent to those of WT mice. The PaO₂ levels began to decrease at the age of 30 wk and dropped further at 35 wk (Fig. 1 f). Similar pulmonary fibrosis was also observed in mice in which the point mutation was inserted using the CRISPR-Cas9 method (Fig. S2 b). These data demonstrated that the *Sftpa1* mutation in mice caused spontaneous pulmonary fibrosis at 20 wk of age with further deterioration with aging. This finding strongly suggested that the corresponding mutation in human *SFTPA1* found in the study family was the causative mutation for IPF in these cases.

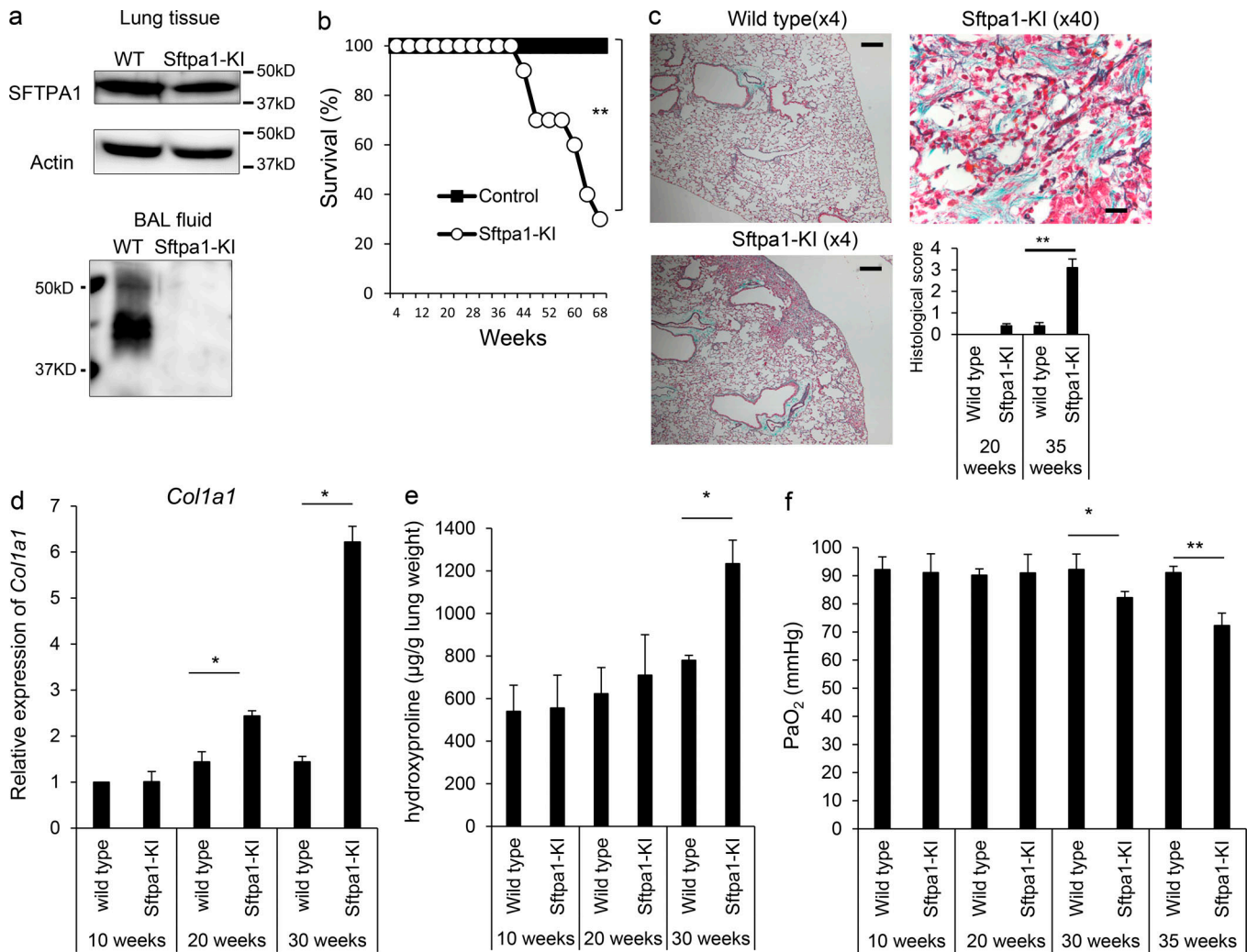


Figure 1. Sftpa1-KI mice spontaneously developed pulmonary fibrosis. (a) Western blot analysis of Sftpa1 in lung tissue or BAL fluid of WT or Sftpa1-KI mice. (b) Survival analysis of WT (closed squares) or Sftpa1-KI mice (open circles; number of mice in each independent experiment is 20). **, $P < 0.01$ by log-rank test. (c) Representative image of Masson's trichrome-staining (4 \times for WT and Sftpa1-KI [the scale bar indicates 200 μ m] and 40 \times for Sftpa1-KI mice [the scale bar indicates 20 μ m]) of lung sections from WT or Sftpa1-KI mice at the age of 35 wk and their pathological score. Data are means \pm SD. **, $P < 0.01$. (d and e) Quantification of mRNA of *Col1a1* (d) and hydroxyproline contents (e) in WT or Sftpa1-KI mice (number of mice in each independent experiment is seven) at the indicated age. (f) Measurement of arterial PaO₂ in WT or Sftpa1-KI mice (number of mice in each independent experiment is seven) at the indicated age. Data (d–f) are means \pm SD. *, $P < 0.05$; **, $P < 0.01$. Data shown are representative of four (b–e) independent experiments or cumulative of three (f) independent experiments.

Influenza virus infection accelerated pulmonary fibrosis in Sftpa1-KI mice

To evaluate the molecular mechanism underlying pulmonary fibrosis in Sftpa1-KI mice, we infected them with influenza A virus (IAV) because lung infection is known to worsen clinical symptoms in IPF patients (Moua et al., 2016). Both control and Sftpa1-KI mice at the age of 20 wk showed similar virus titers in the lungs 3–12 d after IAV infection (Fig. S2 c). The virus was eradicated 12 d after infection (Fig. S2 c). This demonstrated that the *Sftpa1* mutation did not affect susceptibility to IAV infection. However, Sftpa1-KI mice began to die 13 d after infection, and by 28 d, ~70% of the mice had died (Fig. 2 a). The control and Sftpa1-KI mice had similar total cell numbers 3 and 7 d after infection (Fig. 2 b). The lung histopathology of IAV-infected Sftpa1-KI mice showed pulmonary fibrosis with cellular

infiltration 10 d after infection with high pathological score, whereas the control lungs showed little sign of pulmonary fibrosis (Fig. 2 c). Lung hydroxyproline was higher in Sftpa1-KI mice than in control mice (Fig. 2 d). In addition, the level of matrix metalloproteinase-9 in the BAL fluid was increased in aged Sftpa1-KI mice as well as in IAV-infected Sftpa1-KI mice (Fig. 2 e).

Influenza virus infection accelerated pulmonary fibrosis in Sftpa1-KI mice

As epithelial cell death is involved in pulmonary fibrosis (Farkas et al., 2011), we tested for the death of AEII cells in Sftpa1-KI mice. In Sftpa1-KI mice, more AEII cells were positive for 7-aminoactinomycin D (7AAD) after infection with IAV. This was more evident at 30 wk of age than 10 wk of age (Fig. 3 a).

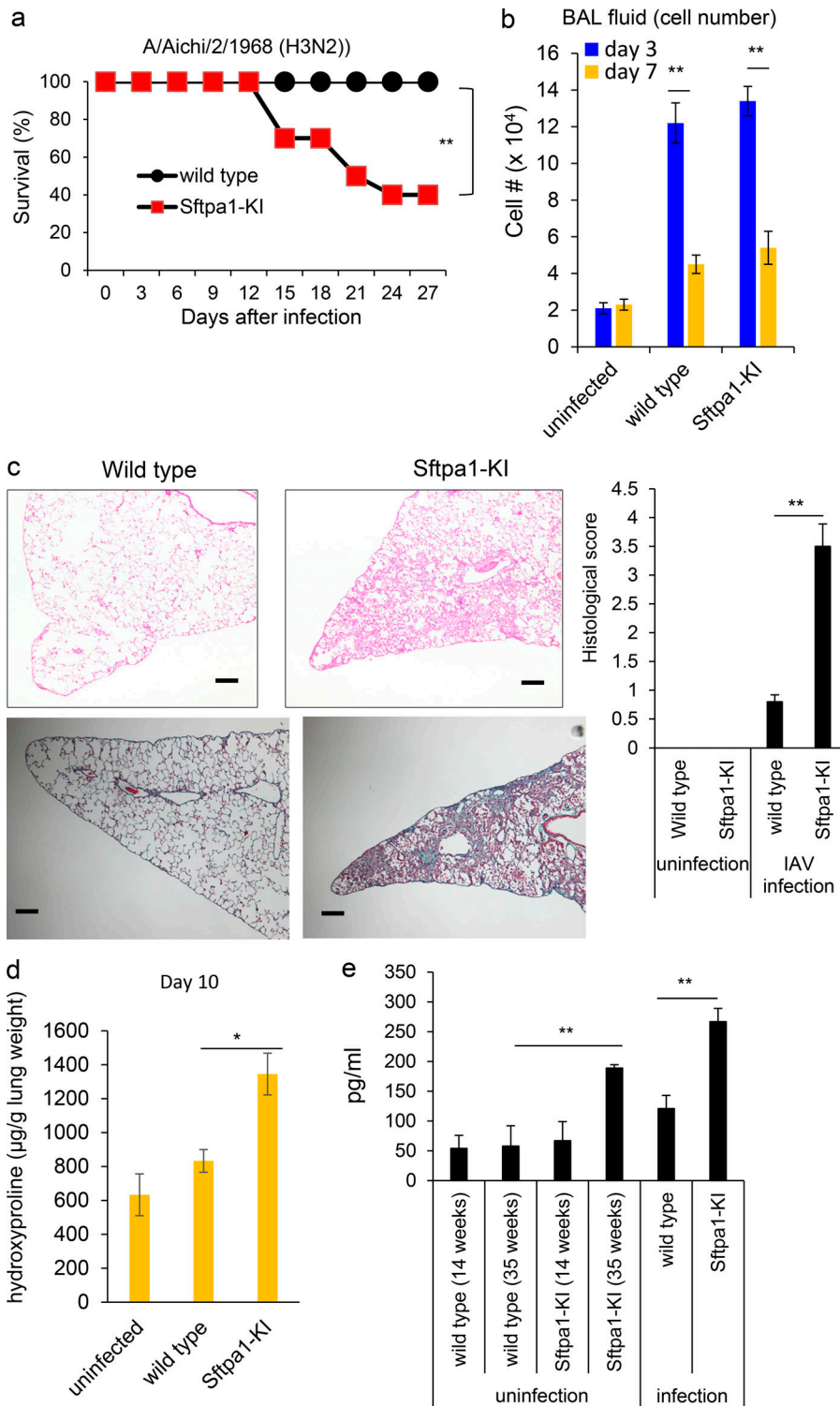


Figure 2. Infection with IAV accelerated the development of pulmonary fibrosis in *Sftpa1-KI* mice. (a) Survival analysis of WT (closed circles) or *Sftpa1-KI* (red squares) mice at the age of 20 wk after IAV infection (number of mice in each independent experiment is 10). ***P* < 0.01 by log-rank test. (b) Total cell number in BAL fluid was counted in WT or *Sftpa1-KI* mice (*n* = 10 each) 3 (blue) or 7 (orange) d after IAV infection. Data are means ± SD. ***P* < 0.01. (c) Representative image of Masson's trichrome-staining of lung sections and clinical score from WT or *Sftpa1-KI* mice 10 d after IAV infection. The scale bar indicates 200 μm. Data are means ± SD. ***P* < 0.01. (d) Quantification of hydroxyproline contents in WT or *Sftpa1-KI* mice (number of mice in each independent experiment is 10) 10 d after IAV infection. Data are means ± SD. **P* < 0.05. (e) Matrix metalloprotease-9 levels in the BAL fluid in WT and *Sftpa1-KI* mice at the age of 14 or 35 wk or in IAV-infected WT and *Sftpa1-KI* mice at the age of 20 wk (day 10; ***P* < 0.01; number of mice in each independent experiment is five). Data shown are representative of five (a-c) independent experiments or cumulative of two (d and e) independent experiments.

The number of SP-C-positive cells was also lower in *Sftpa1-KI* than WT mice at the age of 30 wk (Fig. 3 a). These data indicate that AEII cells in *Sftpa1-KI* mice have a tendency to die compared with those in WT mice. The expression of active caspase-3 in the AEII cells of *Sftpa1-KI* mice was equivalent to the WT (Fig. 3 b), suggesting that apoptosis was not involved in the increased cell death in *Sftpa1-KI* mice. We next sought to assess the contribution of necroptosis to cell death. We crossed *Sftpa1-KI* mice

with *Ripk3*-deficient (*Sftpa1-KI*; *Ripk3*^{-/-}) mice and infected the resultant offspring with IAV. About 90% of the *Sftpa1-KI*; *Ripk3*^{-/-} mice survived after IAV infection, although >60% of control *Sftpa1-KI* mice died after infection (Fig. 3 c). The accumulation of hydroxyproline was also less in *Sftpa1-KI*; *Ripk3*^{-/-} mice than in control mice (Fig. 3 c). In *Sftpa1-KI*; *Ripk3*^{-/-} mice, the number of AEII cells positive for 7AAD after infection with IAV was equivalent to the WT (Fig. 3 d). The *Sftpa1-KI*; *Ripk3*^{-/-}

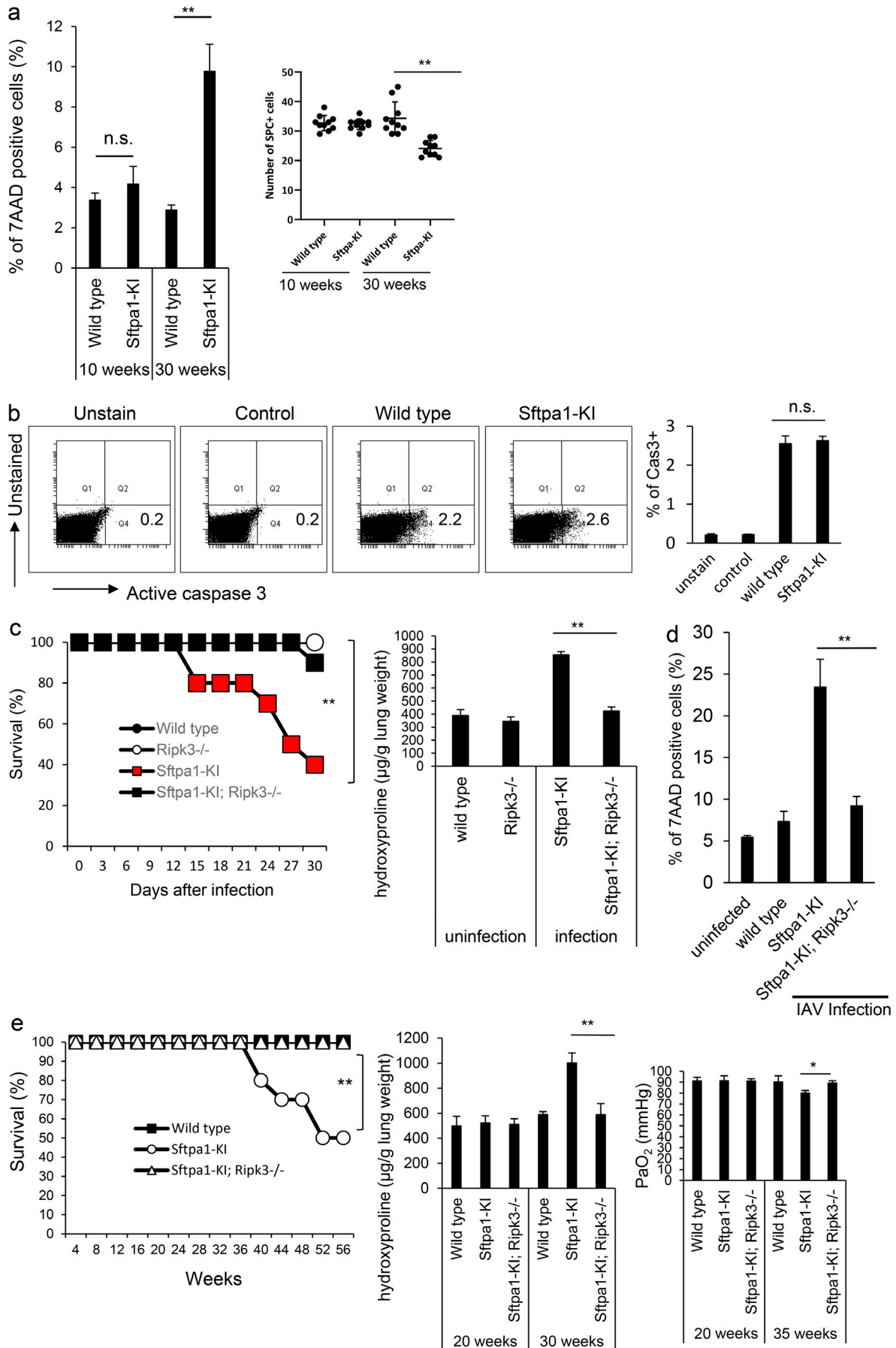


Figure 3. Increased necroptosis of AEII cells in Sftpa1-KI mice. (a) The percentage of 7AAD-positive cells (at the ages of 10 or 30 wk) in AEII cells or SP-C-positive cells (average of the number of SP-C-positive cells in 10 independent fields in right lung) was counted (number of mice in each independent experiment is 10). Data are means \pm SD. n.s., not significant; **, $P < 0.01$. (b) The expression of active caspase-3 (at the age of 30 wk) from WT or Sftpa1-KI mice 10 d after IAV infection. As a negative control, unstained sample was prepared, and isotype-matched antibodies were used to stain WT cells (control). The number in each figure indicates the percentage of active caspase-3-positive cells. Data are means \pm SD. (c) Survival of WT (closed circles), Ripk3^{-/-} (open circles), Sftpa1-KI (red squares), or Sftpa1-KI; Ripk3^{-/-} (closed squares) mice after IAV infection (number of mice in each independent experiment is 10). **, $P < 0.01$ by log-rank test. Quantification of hydroxyproline contents in control, Ripk3^{-/-}, Sftpa1-KI, or Sftpa1-KI; Ripk3^{-/-} mice (number of mice in each independent experiment is 10) 12 d after IAV infection. Data represent the means \pm SD. **, $P < 0.01$. (d) The percentage of 7AAD-positive cells in AEII cells from WT, Sftpa1-KI, or Sftpa1-KI; Ripk3^{-/-} mice 10 d after IAV infection. Data are means \pm SD. **, $P < 0.01$. (e) Survival of WT (closed squares), Sftpa1-KI (open circles), or Sftpa1-KI; Ripk3^{-/-} (open triangles) mice after IAV infection (number of mice in each independent experiment is 20). **, $P < 0.01$ by log-rank test. Quantification of hydroxyproline contents or measurement of arterial PaO₂ in WT, Sftpa1-KI, or Sftpa1-KI; Ripk3^{-/-} mice (number of mice in each independent experiment is seven) at the indicated age. Data are means \pm SD. *, $P < 0.05$; **, $P < 0.01$. The data in this figure are representative of four independent experiments. Data shown are representative of five (c–e) independent experiments or cumulative of five (a and b) independent experiments.

mice did not die during the first 56 wk of life (Fig. 3 e). The deletion of *Ripk3* led to the reduction of hydroxyproline accumulation and recovered PaO₂ level in Sftpa1-KI mice (Fig. 3 e). Moreover, deletion of *Mlkl* in Sftpa1-KI mice also showed resistance to pulmonary fibrosis after IAV infection (Fig. S2 d). These data suggest that increased necroptosis was responsible for Sftpa1-KI mouse death.

To assess whether necroptosis was enhanced in IPF patients with *SFTPA1* mutations, we evaluated a patient's expression of phosphorylated MLKL. Although we could assess a lung specimen from only one patient, we detected increased levels of phosphorylated MLKL expression in AEII cells of the IPF patient (Fig. S2 e). Phosphorylated MLKL was not detected in control lung tissue and other IPF patients without *SFTPA1* mutation (Fig. S2 e).

Increased ER stress and JNK activation contributed to IPF

As the secretion but not intracellular expression of Sftpa1 was disturbed in Sftpa1-KI mice, we sought to determine whether ER stress was induced in Sftpa1-KI mice. We tested the phosphorylation of IRE1 α in AEII cells from control and Sftpa1-KI mice infected with IAV. The infected AEII cells from Sftpa1-KI mice showed increased phosphorylation of IRE1 α compared with WT mice 10 d after infection (Fig. 4 a). However, we did not find differences in phosphorylated eIF2 α expression (Fig. S3 a). Up-regulated phosphorylation of IRE1 α was detected even in uninfected Sftpa1-KI mice at the age of 20 wk (Fig. 4 a). The phosphorylation of IRE1 α activates and phosphorylates JNK (Sano and Reed, 2013). Therefore, we measured phosphorylated JNK levels in AEII cells from Sftpa1-KI mice infected with IAV (Fig. 4 b). The AEII cells from Sftpa1-KI mice showed increased phosphorylation of JNK (Fig. 4 b and Fig. S3 b), and its phosphorylation was suppressed by blockade of IRE1 α (Fig. 4 b). The increased phosphorylation of JNK was detected in AEII cells in Sftpa1-KI mice infected with IAV (Fig. S3 c). To determine whether JNK activation was involved in lung fibrosis in Sftpa1-KI mice, we treated Sftpa1-KI mice with a JNK inhibitor. The JNK inhibitor ameliorated lung fibrosis in Sftpa1-KI mice, although less efficiently than deleting the *Ripk3* gene (Fig. 4 c).

To evaluate the association of the IRE1 α -JNK pathway with necroptosis, we evaluated the expression of Ripk3 in AEII cells. We detected increased expression of Ripk3 in Sftpa1-KI compared with WT mice infected with IAV (Fig. 4 d). Treatment

with a JNK inhibitor reduced Ripk3 expression in Sftpa1-KI mice (Fig. 4 d), indicating that Ripk3 expression is regulated by JNK activation. This dose of JNK inhibitor clearly suppressed LPS-induced TNF- α production in mice (Fig. S3 d). In addition, even in the absence of IAV infection, Ripk3 expression was higher in Sftpa1-KI than WT mice at the age of 20 wk (Fig. 4 d). In addition, although we tried to detect phosphorylated MLKL (pMLKL) and IRE1 α in situ, we have not been able to detect any specific staining of each molecule in situ by using commercially available antibodies.

Increased Ripk3 expression contributes to IPF

Finally, we analyzed whether increased Ripk3 expression induced by JNK activation was responsible for pulmonary fibrosis in Sftpa1-KI mice. We constructed an adenovirus vector encoding *Ripk3* (Ripk3-adenovirus). The intratracheal infection of Ripk3-adenovirus in WT mice led to overexpression of Ripk3-adenovirus in the lung (Fig. 5 a). The infection of Ripk3-adenovirus reduced the survival of Sftpa1-KI mice that were infected with IAV and treated with a JNK inhibitor (Fig. 5 b and Fig. S3 e), demonstrating that JNK-mediated Ripk3 expression is, at least partly, responsible for the pulmonary fibrosis in Sftpa1-KI mice. The overexpression of Ripk3 in WT mice infected with IAV also showed pulmonary fibrosis, although it was less than in Sftpa1-KI mice infected with IAV.

Here, we identified a homozygous mutation in *SFTPA1* in IPF patients from a consanguineous Japanese family. We demonstrated that mice carrying the same mutation in *Sftpa1* spontaneously developed pulmonary fibrosis that was accelerated by IAV infection. ER stress was induced in AEII cells in Sftpa1-KI mice, resulting in activation of the JNK-Ripk3 pathway. Previous studies have reported the presence of highly activated JNK in IPF- and bleomycin-instilled lung tissue samples, and overexpression of caveolin-1 was able to suppress JNK (Wang et al., 2006). JNK signaling in AEII cells up-regulated Ripk3 expression, leading to an increased sensitivity to necroptosis in AEII cells, which contributed to the development of pulmonary fibrosis. These studies identified necroptosis of AEII cells as the crucial event in pulmonary fibrosis, illustrating the potential utility of targeting necroptosis in the treatment of IPF.

Earlier studies in IPF patients demonstrated epithelial cell loss and increased epithelial cell death, including apoptosis and necrosis (Uhal et al., 1998; Tanjore et al., 2012). Subsequent

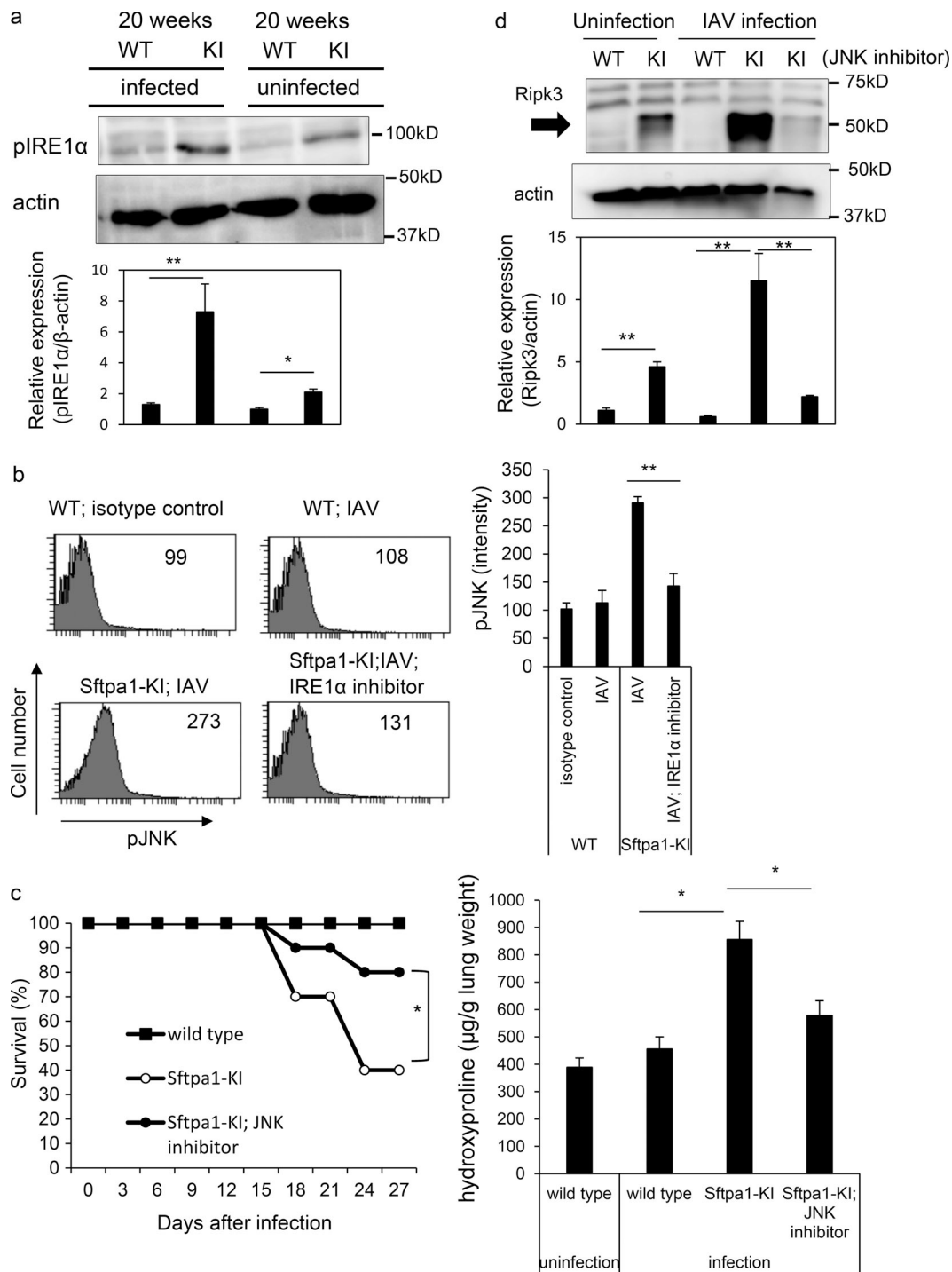


Figure 4. **Enhanced ER stress in AEII cells from Sftpa1-KI mice.** (a) Western blot showing levels of phosphorylated IRE1α and actin in AEII cells of 20-wk-old WT and Sftpa1-KI (KI) mice 7 d after infection with IAV or uninfected WT and KI mice at 20 wk of age. Data represent the means ± SD. *, P < 0.05; **, P < 0.01. (b) Flow cytometric analysis of phosphorylated JNK in WT mice, day 7 IAV-infected Sftpa1-KI or WT mice, or Sftpa1-KI mice infected with IAV and treated with IRE1α inhibitor. Data represent the means ± SD. **, P < 0.01. (c) Survival of WT (closed squares), Sftpa1-KI (open circles), or Sftpa1-KI (closed circles) mice at the age of 20 wk treated with a JNK inhibitor after IAV infection (number of mice in each independent experiment is 10). *, P < 0.05 by log-rank test. Quantification of hydroxyproline contents in WT or Sftpa1-KI mice (number of mice in each independent experiment is 10) 12 d after IAV infection. Data represent the means ± SD. *, P < 0.05. (d) RIPK3 expression in AEII cells in 20-wk-old WT and Sftpa1-KI mice, 20-wk-old WT and Sftpa1-KI mice 7 d after infection with IAV, and 20-wk-old KI mice 7 d after infection with IAV and treated with a JNK inhibitor. Data represent the means ± SD. **, P < 0.01. Data shown are representative of five (c and d) independent experiments or cumulative of five (a and b) independent experiments.

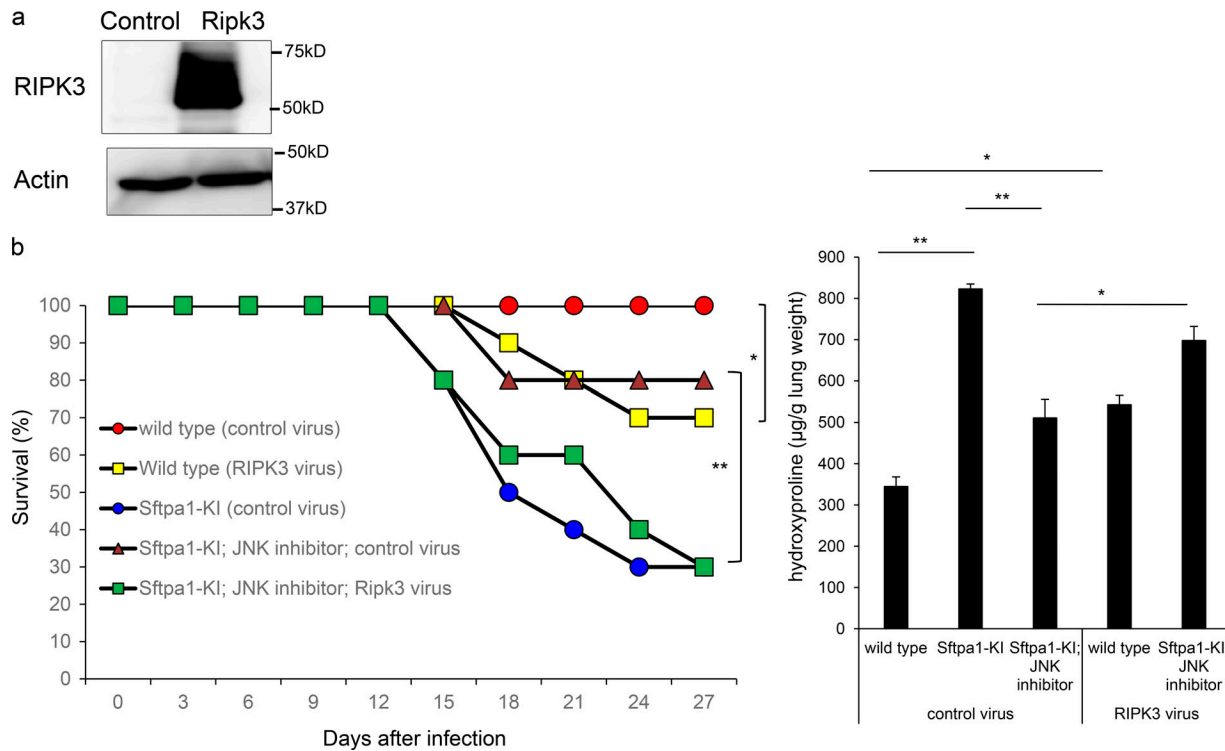


Figure 5. Up-regulation of Ripk3 contributed to IPF development in Sftpa1-KI mice. (a) Western blot analysis of the levels of Ripk3 and β -actin in WT mice infected with control adenovirus or adenovirus carrying Ripk3. **(b)** Survival of 20-wk-old WT (red circles), WT infected with adenovirus carrying Ripk3 (yellow squares), Sftpa1-KI mice infected with control virus (blue circles), Sftpa1-KI mice infected with control virus and treated with a JNK inhibitor (brown triangles), or Sftpa1-KI mice infected with adenovirus carrying Ripk3 and treated with a JNK inhibitor (green squares; number of mice in each independent experiment is 10). *, $P < 0.05$; **, $P < 0.01$ by log-rank test. Quantification of hydroxyproline contents in WT or Sftpa1-KI mice (number of mice in each independent experiment is 10) 12 d after IAV infection. Data represent the means \pm SD. *, $P < 0.05$; **, $P < 0.01$ by multiple testing corrections. Data shown are representative of three (b) independent experiments.

studies suggested that repeated epithelial injury led to a highly aberrant wound healing response that contributed to IPF pathogenesis (Datta et al., 2011). Indeed, increased TUNEL or cleaved caspase-3-positive cells in lung tissue from IPF patients suggested the involvement of apoptosis in IPF pathogenesis (Korfei et al., 2008). The most widely used animal model for IPF is bleomycin-induced pulmonary fibrosis, which is caused by injury and cell death of alveolar epithelial cells. A caspase inhibitor can ameliorate bleomycin-induced pulmonary fibrosis (Kuwano et al., 2001), suggesting that apoptosis is involved in pulmonary fibrosis in this model. However, it remains unclear if apoptosis or necrosis is directly involved in the onset or progression of human IPF. Our current data demonstrate that necroptosis is the crucial cell death pathway that causes IPF in the family reported here and potentially in others with a similar mutation. This is supported by the deletion of *Ripk3* or *Mlkl* that could suppress the development of IPF in Sftpa1-KI mice, although we need to establish a more refined system, such as the deletion of either gene in only AEII cells, to more fully confirm this hypothesis in future studies. Necroptosis acts as a mediator for pathogen defense and inflammation (Pasparakis and Vandenabeele, 2015). Unlike apoptosis, which is considered to be nonimmunogenic, dying cells that undergo necrosis or necroptosis release damage-associated molecular patterns believed to trigger inflammation. There are several studies that implicate necroptosis in tissue

inflammation in animal models (Bonnet et al., 2011; Welz et al., 2011; Wu et al., 2013). However, there is no evidence that necroptosis is directly involved in human diseases. In this regard, our study is the first to establish a link between necroptosis and inherited IPF and paves the way for future work to examine the contribution of necroptosis to human inflammatory diseases. Although the subsequent molecular cascades or cellular interactions after necroptosis of AEII cells have yet to be determined, our study suggests that blocking necroptosis in AEII cells should suppress the very early events that lead to pulmonary fibrosis in IPF patients.

The activation of RIPK1 leads to cell death through the formation of a RIPK1-TRADD-FADD-caspase-8 complex (Shan et al., 2018; Yuan et al., 2019). This complex triggers caspase activation and causes RIPK1-dependent apoptosis. When caspase activity is deficient in this situation, RIPK1 activation leads to necroptosis through the formation of a RIPK1-RIPK3-MLKL complex in which phosphorylation of MLKL by RIPK3 leads to disruption of the cell membrane and cell lysis (Yuan et al., 2019). Moreover, RIPK3 regulates not only necroptosis but also other cellular responses independent of MLKL. For instance, RIPK3 regulates kidney fibrosis via AKT-dependent ATP citrate lyase (Imamura et al., 2018). In the present study, although we did not evaluate the roles of RIPK1, deletion of *Ripk3* or *Mlkl* suppressed the progression of pulmonary fibrosis in Sftpa1-KI mice,

demonstrating that RIPK3-mediated MLKL activation is a crucial determinant for pulmonary fibrosis in *Sftpa1*-KI mice. The question remains as to which upstream pathways activate RIPK3 in *Sftpa1*-KI mice. The overexpression of RIPK3 in WT mice infected with IAV showed pulmonary fibrosis, although less so than *Sftpa1*-KI mice, which suggests that high expression of RIPK3 may be a key determinant in the increased susceptibility for necroptosis in AEII cells. The improved survival in WT mice in which RIPK3 is overexpressed compared with *Sftpa1*-KI mice infected with IAV could be attributed to the presence of key upstream factors that trigger RIPK3 in *Sftpa1*-KI mice, the presence of RIPK3-independent pathways to increase the susceptibility to necroptosis in *Sftpa1*-KI mice, or the incomplete adenoviral mediated-overexpression of RIPK3 in all parts of the lung.

Our data demonstrate that necroptosis is one of the crucial initiators of pulmonary fibrosis. Therefore, the signaling pathway of necroptosis could be a potential target for its treatment. The current focus for treating IPF is to block the activation of kinases in fibrotic regions involved in IPF progression (Richeldi et al., 2011, 2014; King et al., 2014). In contrast, the modulation of necroptosis in AEII cells would suppress earlier events in IPF progression, which would be more beneficial to patients. Our data thus provide not only a new link between necroptosis and IPF, but also a novel strategy for treating patients with IPF.

Materials and methods

Patients and ethics

All genetic studies were conducted after obtaining informed consent from the patients or the patients' relatives (if patients were deceased). The studies were approved by the human genome research and clinical studies ethics committee of Tokushima University. This study was conducted in accordance with the principles of the Declaration of Helsinki.

Exome resequencing and DNA sequencing

Exome sequencing and data analysis were performed as described previously (Kitamura et al., 2011, 2014). Briefly, a paired-end library was prepared from genomic DNA and hybridized to biotinylated complementary RNA oligonucleotide baits from the SureSelect Human All Exon Kit (Agilent Technologies). The library was sequenced with paired-end, 75-bp reads on one lane of an Illumina HiSeq 1500 sequencing system. The sequence reads were aligned to the human reference sequence of the UCSC Genome Browser (hg19). 90% of the entire targeted exome was covered by >10 reads. DNA variants located in the candidate region were filtered against the databases of the Single Nucleotide Polymorphism Database build 134, the 1000 Genomes Project, and the National Heart, Lung, and Blood Institute Exome Sequencing Project. Missense, nonsense, frameshift, and splice-site alleles were evaluated. The mutation in *SFTPA1* was sequenced using an ABI Prism 3100 genetic analyzer (PE Applied Biosystems).

Single nucleotide polymorphism homozygosity mapping and linkage analysis

Both affected and unaffected siblings from one consanguineous family were studied with the Illumina Human 610 Quad Bead

Chip. Sample processing and labeling were performed in accordance with the manufacturer's instructions. An average call rate of >99% was obtained. Homozygous regions were identified using HomozygosityMapper (Seelow et al., 2009). Our laboratory has developed a graphic interface that allows an easy comparison of common homozygous regions between three patients from different families. For linkage analysis, multi-point log of the odds ratio scores were obtained using Merlin software (Abecasis et al., 2002).

Mice

C57BL/6 mice were purchased from Japan SLC. *Sftpa1*-KI mice were established by constructing a targeting vector with a mutation in *Sftpa1* or putting a mutation in *Sftpa1* in the CRISPR/Cas9 method. All mice, including *Ripk3*^{-/-}, *Mlkl*^{-/-}, and *Sftpa1*-KI mice, were maintained in the animal research center of Tokushima University, and all animal experiments were approved by the animal research committee of Tokushima University and performed in accordance with our institution's guidelines for animal care and use.

BAL

Mice were euthanized, and lung tissue and BAL fluids were collected using 0.8-ml aliquots of PBS. Cell-free BAL fluids were stored in a -80°C freezer before analysis.

Flow cytometry

Cells were resuspended in staining buffer, incubated with anti-*Fcγ*RIII/III mAbs (2.4G2) before staining. AEII cells were characterized as granular cells with high side scatter that expressed Ep-CAM (anti-CD326 mAb, clone G8.8; BioLegend) and were negative for CD45, CD11b, CD11c, CD31, and podoplanin. Phosphorylated JNK was stained with anti-phosphorylated JNK (pJNK) antibody (N9-66; BD Biosciences). Active caspase was stained with Caspase-3 Assay Kit, PhiPhiLux-G2D2. The fluorescence intensity of 10⁵ cells was measured with a FACSCanto II flow cytometer (BD Biosciences) and analyzed with FACSDiva (BD Biosciences) software.

Western blotting and immunoprecipitation

Cell pellets were lysed in cold radioimmunoprecipitation assay buffer (Wako Pure Chemical Industries) and protease inhibitor (Roche), and the lysates were boiled in SDS loading dye. The samples were resolved by SDS-PAGE, and the blots were incubated with anti-Flag (F1804; Sigma-Aldrich), anti-Myc (9E10; Santa Cruz), anti-phospho-IRE1α (rabbit polyclonal antibody; Novus Biologicals), anti-JNK (#9252; Cell Signaling Technology), anti-pJNK (#9251; Cell Signaling Technology), anti-phosphorylated-eIF2α (#9721; Cell Signaling Technology), eIF2α (#5324; Cell Signaling Technology), or anti-Ripk3 (rabbit polyclonal antibody, NBP1-77299; Novus Biologicals) antibodies. They were next incubated with peroxidase-conjugated goat anti-mouse IgG (31430; Pierce Biotechnology) or goat anti-rabbit IgG (170-6515; Bio-Rad) antibodies. As a control, membranes were probed with polyclonal anti-actin (A2066; Sigma-Aldrich) and HRP-conjugated goat anti-rabbit IgG antibodies (170-6515; Bio-Rad). The bands were detected with ECL Prime Chemiluminescent

Substrate (GE Healthcare) and with the ImageQuant LAS-4000 mini system (GE Healthcare).

For immunoprecipitation analysis, FLAG or Myc-tagged human SFTPA1 or SFTPA2 cDNAs were cloned in pcDNA and transfected into A549 cells with GeneJuice (Merck). One day after transfection, the cells were washed three times with serum-free medium and then incubated in serum-free medium for 1 d. The supernatant was subjected to immunoprecipitation with anti-FLAG antibody clone M2 (Sigma-Aldrich) and Dynabeads Protein G (Thermo Fisher Scientific). The cells were washed with PBS, lysed in RIPA buffer (Wako) and subjected to immunoprecipitation in the same manner as the supernatant. The immunoprecipitated samples and total cell lysates were analyzed by Western blotting with anti-FLAG antibody (clone M2) or anti-Myc antibody (clone D84C12).

Measurement of matrix metalloproteinase-9 levels

The concentration of matrix metalloproteinase in BAL fluid from mice was measured with an MMP-9 activity kit (Quickzyme Biosciences).

Real-time PCR

Total RNA was isolated (ReliaPrep RNA Cell Miniprep System; Promega), and cDNA was synthesized (0.1 μ g of RNA). Relative expression was calculated using the comparative threshold cycle method. PCR analyses were performed using StepOnePlus (Applied Biosystems) with primers. Primer sequences are available upon request. The mRNA level of *CypA* was used as an internal control.

Purification of AEII

The lungs were perfused with 5 ml of PBS through the pulmonary artery via the right ventricle. 1 ml of porcine elastase (4.5 U; Roche Diagnostics) was instilled through a tracheal cannula. The lung lobes were gently separated from the bronchi and minced in RPMI 1640 medium containing 20% FBS and 100 U/ml DNase I (Qiagen). Cells in suspension were subsequently filtered through 100-, 70-, and 40- μ m nylon mesh (Corti et al., 1996). Contaminating leukocytes, endothelial cells, and alveolar type I epithelial cells were depleted using biotinylated anti-CD45, CD11b, CD11c, CD31, and podoplanin antibodies (BioLegend) and streptavidin paramagnetic microbeads (Miltenyi Biotec; Marsh et al., 2009).

Measurement of hydroxyproline

Hydroxyproline concentrations in lung tissues were measured with a hydroxyproline assay kit (QuickZyme Hydroxyproline Assay; QuickZyme Biosciences). Hydroxyproline content is expressed as “ μ g per lung,” unless specified otherwise.

Histology

Paraffin-embedded sections were used for hematoxylin and eosin or Masson's trichrome staining. Lung sections were stained with hematoxylin and anti-phosphorylated-MLKL (ab187091; Abcam), anti-pJNK (#9251; Cell Signaling Technology), or SP-C (ab90716; Abcam) antibody followed by EnVision Dual Link System-HRP (K4061; Dako), and then visualized with SignalStain DAB Substrate Kit (Cell Signaling Technology). The severity of inflammation and fibrosis was semi-quantitatively assessed according to the

methods proposed by Genovese et al. (2005) and Ashcroft et al. (1988). The pathological grade was determined according to the following criteria: 0, normal; 1, presence of inflammation and fibrosis involving <5% of the lung parenchyma; 2, presence of inflammation and fibrosis involving <25% of the lung parenchyma; 3, lesions involving 25–50% of the lung, moderate thickening of the bronchial wall without obvious damage to lung architecture, or small fibrous masses; 4, lesions involving >50% of the lung, definite damage to lung structure, and formation of fibrous bands or small fibrous masses; and 5, lesions involving >50% of the lung, severe distortion of structure, and fibrous obliteration of fields.

Influenza infection

Mice (20 wk old) were anesthetized and inoculated intranasally with influenza virus (H3N2; Kashima et al., 2009) in 20 μ l sterile PBS. The titer was measured as described previously (Kashima et al., 2009). The survival of infected mice was observed daily. In other experiments, mice were intravenously treated with a JNK inhibitor (SP600125; Cell Signaling Technology; 30 mg/kg, s.c.; day 0: infection; days 5, 7, 9, and 11), or treated with IRE1 α inhibitor (KIRA6; Thermo Fisher Scientific; 10 mg/kg, intratracheally; day 0: infection; days 3, 5, 7, and 9).

Pulmonary function measurements

The i-STAT Portable Clinical Analyzer and the i-STAT G7+ cartridge were used to measure arterial blood gas (Abbott Point of Care). The arterial blood sampled from the left ventricle of the mice was introduced into the sample well of the cartridge that was subsequently inserted into the analyzer. The PaO₂ was measured after completion of the calibration.

Adenovirus infection

The recombinant E1-deleted adenoviral vectors carrying mouse *Ripk3* under cytomegalovirus promoters were generated and purified. Mice were infected with the recombinant adenovirus by intratracheally injecting 10⁹ PFU/mouse 1 d after IAV infection as previously described (Nakao et al., 1999).

Statistics

The statistical significance of between-group differences was evaluated by an unpaired test, a two-tailed *t* test, a parametric Dunnett's test, or a log-rank test. A *P* value < 0.05 was considered significant.

Online supplemental material

Fig. S1 shows the genetic analysis of IPF patients and the effect of the mutation in *SFTPA1* on its protein function. Fig. S2 shows the development of pulmonary fibrosis in *Sftpa1*-KI mice. This relates to Figs. 1, 2, and 3. Fig. S3 shows the contribution of the JNK pathway in the development of pulmonary fibrosis in *Sftpa*-KI mice. This relates to Figs. 4 and 5.

Acknowledgments

We thank Dr. Y. Itoh (Shiga Medical University, Otsu, Japan) for providing influenza virus, and Ms. C. Kinouchi, K. Takahashi, Y. Shinomiya, and A. Kitamura for their technical assistance.

This work was supported by JSPS KAKEN grant numbers JP16K09957 (to Y. Setoguchi) and JP26110008 (to K. Yasutomo), Practical Research Project for Rare/Intractable Diseases in AMED (to Y. Setoguchi), and AMED-CREST (to K. Yasutomo).

The authors declare no competing financial interests.

Author contributions: A. Takezaki, S. Tsukumo, and K. Yasutomo designed the experiments. A. Takezaki, S. Tsukumo, and K. Yasutomo performed the experiments. A. Takezaki, S. Tsukumo, H. Goto, K. Hosomichi, H. Uehara, Y. Setoguchi, Y. Nishioka, and K. Yasutomo analyzed the data. J.G. Ledford prepared reagents. A. Takezaki, S. Tsukumo, and K. Yasutomo wrote the manuscript. K. Yasutomo supervised all experiments.

Submitted: 19 December 2018

Revised: 29 April 2019

Accepted: 6 September 2019

References

- Abecasis, G.R., S.S. Cherny, W.O. Cookson, and L.R. Cardon. 2002. Merlin-rapid analysis of dense genetic maps using sparse gene flow trees. *Nat. Genet.* 30:97–101. <https://doi.org/10.1038/ng786>
- Ahluwalia, N., B.S. Shea, and A.M. Tager. 2014. New therapeutic targets in idiopathic pulmonary fibrosis. Aiming to rein in runaway wound-healing responses. *Am. J. Respir. Crit. Care Med.* 190:867–878. <https://doi.org/10.1164/rccm.201403-0509PP>
- Armanios, M. 2013. Telomeres and age-related disease: how telomere biology informs clinical paradigms. *J. Clin. Invest.* 123:996–1002. <https://doi.org/10.1172/JCI66370>
- Ashcroft, T., J.M. Simpson, and V. Timbrell. 1988. Simple method of estimating severity of pulmonary fibrosis on a numerical scale. *J. Clin. Pathol.* 41:467–470. <https://doi.org/10.1136/jcp.41.4.467>
- Bonnet, M.C., D. Preukschat, P.S. Welz, G. van Loo, M.A. Ermolaeva, W. Bloch, I. Haase, and M. Pasparakis. 2011. The adaptor protein FADD protects epidermal keratinocytes from necroptosis in vivo and prevents skin inflammation. *Immunity.* 35:572–582. <https://doi.org/10.1016/j.immuni.2011.08.014>
- Corti, M., A.R. Brody, and J.H. Harrison. 1996. Isolation and primary culture of murine alveolar type II cells. *Am. J. Respir. Cell Mol. Biol.* 14:309–315. <https://doi.org/10.1165/ajrcmb.14.4.8600933>
- Datta, A., C.J. Scotton, and R.C. Chambers. 2011. Novel therapeutic approaches for pulmonary fibrosis. *Br. J. Pharmacol.* 163:141–172. <https://doi.org/10.1111/j.1476-5381.2011.01247.x>
- Farkas, L., J. Gauldie, N.F. Voelkel, and M. Kolb. 2011. Pulmonary hypertension and idiopathic pulmonary fibrosis: a tale of angiogenesis, apoptosis, and growth factors. *Am. J. Respir. Cell Mol. Biol.* 45:1–15. <https://doi.org/10.1165/ajrcmb.2010-0365TR>
- Galluzzi, L., and G. Kroemer. 2008. Necroptosis: a specialized pathway of programmed necrosis. *Cell.* 135:1161–1163. <https://doi.org/10.1016/j.cell.2008.12.004>
- Genovese, T., S. Cuzzocrea, R. Di Paola, E. Mazzone, C. Mastruzzo, P. Catalano, M. Sortino, N. Crimi, A.P. Caputi, C. Thiemermann, and C. Vancheri. 2005. Effect of rosiglitazone and 15-deoxy- $\Delta^{12,14}$ -prostaglandin J_2 on bleomycin-induced lung injury. *Eur. Respir. J.* 25:225–234. <https://doi.org/10.1183/09031936.05.00049704>
- He, S., Y. Liang, F. Shao, and X. Wang. 2011. Toll-like receptors activate programmed necrosis in macrophages through a receptor-interacting kinase-3-mediated pathway. *Proc. Natl. Acad. Sci. USA.* 108:20054–20059. <https://doi.org/10.1073/pnas.1116302108>
- Imamura, M., J.S. Moon, K.P. Chung, K. Nakahira, T. Muthukumar, R. Shingarev, S.W. Ryter, A.M. Choi, and M.E. Choi. 2018. RIPK3 promotes kidney fibrosis via AKT-dependent ATP citrate lyase. *JCI Insight.* 3: 94979. <https://doi.org/10.1172/jci.insight.94979>
- Kashima, Y., M. Ikeda, Y. Itoh, Y. Sakoda, T. Nagata, T. Miyake, K. Soda, H. Ozaki, M. Nakayama, H. Shibuya, et al. 2009. Intranasal administration of a live non-pathogenic avian H5N1 influenza virus from a virus library confers protective immunity against H5N1 highly pathogenic avian influenza virus infection in mice: comparison of formulations and administration routes of vaccines. *Vaccine.* 27:7402–7408. <https://doi.org/10.1016/j.vaccine.2009.08.089>
- King, T.E. Jr., P.W. Noble, and W.Z. Bradford. 2014. Treatments for idiopathic pulmonary fibrosis. *N. Engl. J. Med.* 371:783–784.
- Kitamura, A., Y. Maekawa, H. Uehara, K. Izumi, I. Kawachi, M. Nishizawa, Y. Toyoshima, H. Takahashi, D.M. Standley, K. Tanaka, et al. 2011. A mutation in the immunoproteasome subunit PSMB8 causes autoinflammation and lipodystrophy in humans. *J. Clin. Invest.* 121: 4150–4160. <https://doi.org/10.1172/JCI58414>
- Kitamura, A., Y. Sasaki, T. Abe, H. Kano, and K. Yasutomo. 2014. An inherited mutation in NLRC4 causes autoinflammation in human and mice. *J. Exp. Med.* 211:2385–2396. <https://doi.org/10.1084/jem.20141091>
- Korfei, M., C. Ruppert, P. Mahavadi, I. Henneke, P. Markart, M. Koch, G. Lang, L. Fink, R.M. Bohle, W. Seeger, et al. 2008. Epithelial endoplasmic reticulum stress and apoptosis in sporadic idiopathic pulmonary fibrosis. *Am. J. Respir. Crit. Care Med.* 178:838–846. <https://doi.org/10.1164/rccm.200802-313OC>
- Kuwano, K., R. Kunitake, T. Maeyama, N. Hagimoto, M. Kawasaki, T. Matsuba, M. Yoshimi, I. Inoshima, K. Yoshida, and N. Hara. 2001. Attenuation of bleomycin-induced pneumopathy in mice by a caspase inhibitor. *Am. J. Physiol. Lung Cell. Mol. Physiol.* 280:L316–L325. <https://doi.org/10.1152/ajplung.2001.280.2.L316>
- Li, J., T. McQuade, A.B. Siemer, J. Napetschnig, K. Moriwaki, Y.S. Hsiao, E. Damko, D. Moquin, T. Walz, A. McDermott, et al. 2012. The RIP1/RIP3 necrosome forms a functional amyloid signaling complex required for programmed necrosis. *Cell.* 150:339–350. <https://doi.org/10.1016/j.cell.2012.06.019>
- Maitra, M., Y. Wang, R.D. Gerard, C.R. Mendelson, and C.K. Garcia. 2010. Surfactant protein A2 mutations associated with pulmonary fibrosis lead to protein instability and endoplasmic reticulum stress. *J. Biol. Chem.* 285:22103–22113. <https://doi.org/10.1074/jbc.M110.121467>
- Marsh, L.M., L. Cakarova, G. Kwapiszewska, W. von Wulffen, S. Herold, W. Seeger, and J. Lohmeyer. 2009. Surface expression of CD74 by type II alveolar epithelial cells: a potential mechanism for macrophage migration inhibitory factor-induced epithelial repair. *Am. J. Physiol. Lung Cell. Mol. Physiol.* 296:L442–L452. <https://doi.org/10.1152/ajplung.00525.2007>
- Moriwaki, K., and F.K. Chan. 2013. RIP3: a molecular switch for necrosis and inflammation. *Genes Dev.* 27:1640–1649. <https://doi.org/10.1101/gad.223321.113>
- Moua, T., B.D. Westerly, M.M. Dulohery, C.E. Daniels, J.H. Ryu, and K.G. Lim. 2016. Patients with fibrotic interstitial lung disease hospitalized for acute respiratory worsening: A large cohort analysis. *Chest.* 149: 1205–1214. <https://doi.org/10.1016/j.chest.2015.12.026>
- Nakao, A., M. Fujii, R. Matsumura, K. Kumano, Y. Saito, K. Miyazono, and I. Iwamoto. 1999. Transient gene transfer and expression of Smad7 prevents bleomycin-induced lung fibrosis in mice. *J. Clin. Invest.* 104:5–11. <https://doi.org/10.1172/JCI6094>
- Nathan, N., V. Giraud, C. Picard, H. Nunes, F. Dastot-Le Moal, B. Copin, L. Galaron, A. De Ligniville, N. Kuziner, M. Reynaud-Gaubert, et al. 2016. Germline SFTPA1 mutation in familial idiopathic interstitial pneumonia and lung cancer. *Hum. Mol. Genet.* 25:1457–1467. <https://doi.org/10.1093/hmg/ddw014>
- Noble, P.W., C.E. Barkauskas, and D. Jiang. 2012. Pulmonary fibrosis: patterns and perpetrators. *J. Clin. Invest.* 122:2756–2762. <https://doi.org/10.1172/JCI60323>
- Pasparakis, M., and P. Vandenabeele. 2015. Necroptosis and its role in inflammation. *Nature.* 517:311–320. <https://doi.org/10.1038/nature14191>
- Putman, R.K., I.O. Rosas, and G.M. Hunninghake. 2014. Genetics and early detection in idiopathic pulmonary fibrosis. *Am. J. Respir. Crit. Care Med.* 189:770–778. <https://doi.org/10.1164/rccm.201312-2219PP>
- Raghu, G. 2011. Idiopathic pulmonary fibrosis: increased survival with “gastroesophageal reflux therapy”: fact or fallacy? *Am. J. Respir. Crit. Care Med.* 184:1330–1332. <https://doi.org/10.1164/rccm.201110-1842ED>
- Raghu, G., M. Remy-Jardin, J.L. Myers, L. Richeldi, C.J. Ryerson, D.J. Lederer, J. Behr, V. Cottin, S.K. Danoff, F. Morell, et al. American Thoracic Society, European Respiratory Society, Japanese Respiratory Society, and Latin American Thoracic Society. 2018. Diagnosis of idiopathic pulmonary fibrosis. An official ATS/ERS/JRS/ALAT clinical practice guideline. *Am. J. Respir. Crit. Care Med.* 198:e44–e68. <https://doi.org/10.1164/rccm.201807-1255ST>
- Richeldi, L., U. Costabel, M. Selman, D.S. Kim, D.M. Hansell, A.G. Nicholson, K.K. Brown, K.R. Flaherty, P.W. Noble, G. Raghu, et al. 2011. Efficacy of a tyrosine kinase inhibitor in idiopathic pulmonary fibrosis. *N. Engl. J. Med.* 365:1079–1087. <https://doi.org/10.1056/NEJMoa1103690>

- Richeldi, L., R.M. du Bois, G. Raghu, A. Azuma, K.K. Brown, U. Costabel, V. Cottin, K.R. Flaherty, D.M. Hansell, Y. Inoue, et al. INPULSIS Trial Investigators. 2014. Efficacy and safety of nintedanib in idiopathic pulmonary fibrosis. *N. Engl. J. Med.* 370:2071–2082. <https://doi.org/10.1056/NEJMoa1402584>
- Rickard, J.A., J.A. O'Donnell, J.M. Evans, N. Lalaoui, A.R. Poh, T. Rogers, J.E. Vince, K.E. Lawlor, R.L. Ninnis, H. Anderton, et al. 2014. RIPK1 regulates RIPK3-MLKL-driven systemic inflammation and emergency hematopoiesis. *Cell.* 157:1175–1188. <https://doi.org/10.1016/j.cell.2014.04.019>
- Sano, R., and J.C. Reed. 2013. ER stress-induced cell death mechanisms. *Biochim. Biophys. Acta.* 1833:3460–3470. <https://doi.org/10.1016/j.bbamcr.2013.06.028>
- Seelow, D., M. Schuelke, F. Hildebrandt, and P. Nürnberg. 2009. HomozygosityMapper—an interactive approach to homozygosity mapping. *Nucleic Acids Res.* 37(Web Server issue, suppl):W593–9. <https://doi.org/10.1093/nar/gkp369>
- Seibold, M.A., A.L. Wise, M.C. Speer, M.P. Steele, K.K. Brown, J.E. Loyd, T.E. Fingerlin, W. Zhang, G. Gudmundsson, S.D. Groshong, et al. 2011. A common MUC5B promoter polymorphism and pulmonary fibrosis. *N. Engl. J. Med.* 364:1503–1512. <https://doi.org/10.1056/NEJMoa1013660>
- Shan, B., H. Pan, A. Najafav, and J. Yuan. 2018. Necroptosis in development and diseases. *Genes Dev.* 32:327–340. <https://doi.org/10.1101/gad.312561.118>
- Silke, J., J.A. Rickard, and M. Gerlic. 2015. The diverse role of RIP kinases in necroptosis and inflammation. *Nat. Immunol.* 16:689–697. <https://doi.org/10.1038/ni.3206>
- Steele, M.P., and D.A. Schwartz. 2013. Molecular mechanisms in progressive idiopathic pulmonary fibrosis. *Annu. Rev. Med.* 64:265–276. <https://doi.org/10.1146/annurev-med-042711-142004>
- Sun, L., H. Wang, Z. Wang, S. He, S. Chen, D. Liao, L. Wang, J. Yan, W. Liu, X. Lei, and X. Wang. 2012. Mixed lineage kinase domain-like protein mediates necrosis signaling downstream of RIP3 kinase. *Cell.* 148: 213–227. <https://doi.org/10.1016/j.cell.2011.11.031>
- Tanjore, H., T.S. Blackwell, and W.E. Lawson. 2012. Emerging evidence for endoplasmic reticulum stress in the pathogenesis of idiopathic pulmonary fibrosis. *Am. J. Physiol. Lung Cell. Mol. Physiol.* 302:L721–L729. <https://doi.org/10.1152/ajplung.00410.2011>
- Uhal, B.D., I. Joshi, W.F. Hughes, C. Ramos, A. Pardo, and M. Selman. 1998. Alveolar epithelial cell death adjacent to underlying myofibroblasts in advanced fibrotic human lung. *Am. J. Physiol.* 275:L1192–L1199. <https://doi.org/10.1038/nrm3737>
- Vanden Berghe, T., A. Linkermann, S. Joann-Lanhouet, H. Walczak, and P. Vandenabeele. 2014. Regulated necrosis: the expanding network of non-apoptotic cell death pathways. *Nat. Rev. Mol. Cell Biol.* 15:135–147. <https://doi.org/10.1038/nrm3737>
- Wang, X.M., Y. Zhang, H.P. Kim, Z. Zhou, C.A. Feghali-Bostwick, F. Liu, E. Ifedigbo, X. Xu, T.D. Oury, N. Kaminski, and A.M. Choi. 2006. Caveolin-1: a critical regulator of lung fibrosis in idiopathic pulmonary fibrosis. *J. Exp. Med.* 203:2895–2906. <https://doi.org/10.1084/jem.20061536>
- Wang, Y., P.J. Kuan, C. Xing, J.T. Cronkrite, F. Torres, R.L. Rosenblatt, J.M. DiMaio, L.N. Kinch, N.V. Grishin, and C.K. Garcia. 2009. Genetic defects in surfactant protein A2 are associated with pulmonary fibrosis and lung cancer. *Am. J. Hum. Genet.* 84:52–59. <https://doi.org/10.1016/j.ajhg.2008.11.010>
- Welz, P.S., A. Wullaert, K. Vlantis, V. Kondylis, V. Fernández-Majada, M. Ermolaeva, P. Kirsch, A. Sterner-Kock, G. van Loo, and M. Pasparakis. 2011. FADD prevents RIP3-mediated epithelial cell necrosis and chronic intestinal inflammation. *Nature.* 477:330–334. <https://doi.org/10.1038/nature10273>
- Wu, J., Z. Huang, J. Ren, Z. Zhang, P. He, Y. Li, J. Ma, W. Chen, Y. Zhang, X. Zhou, et al. 2013. Mlkl knockout mice demonstrate the indispensable role of Mlkl in necroptosis. *Cell Res.* 23:994–1006. <https://doi.org/10.1038/cr.2013.91>
- Yoshioka, Y., S. Saiki, Y. Tsutsumi-Ishii, R. Koyama, N. Hirashima, N. Harada, S. Yamasaki, K. Suda, and Y. Fukuchi. 2004. Adult-onset familial pulmonary fibrosis in Japanese brothers. *Pathol. Int.* 54:41–46. <https://doi.org/10.1111/j.1440-1827.2004.01583.x>
- Yuan, J., P. Amin, and D. Ofengeim. 2019. Necroptosis and RIPK1-mediated neuroinflammation in CNS diseases. *Nat. Rev. Neurosci.* 20:19–33. <https://doi.org/10.1038/s41583-018-0093-1>

Supplemental material

Takezaki et al., <https://doi.org/10.1084/jem.20182351>

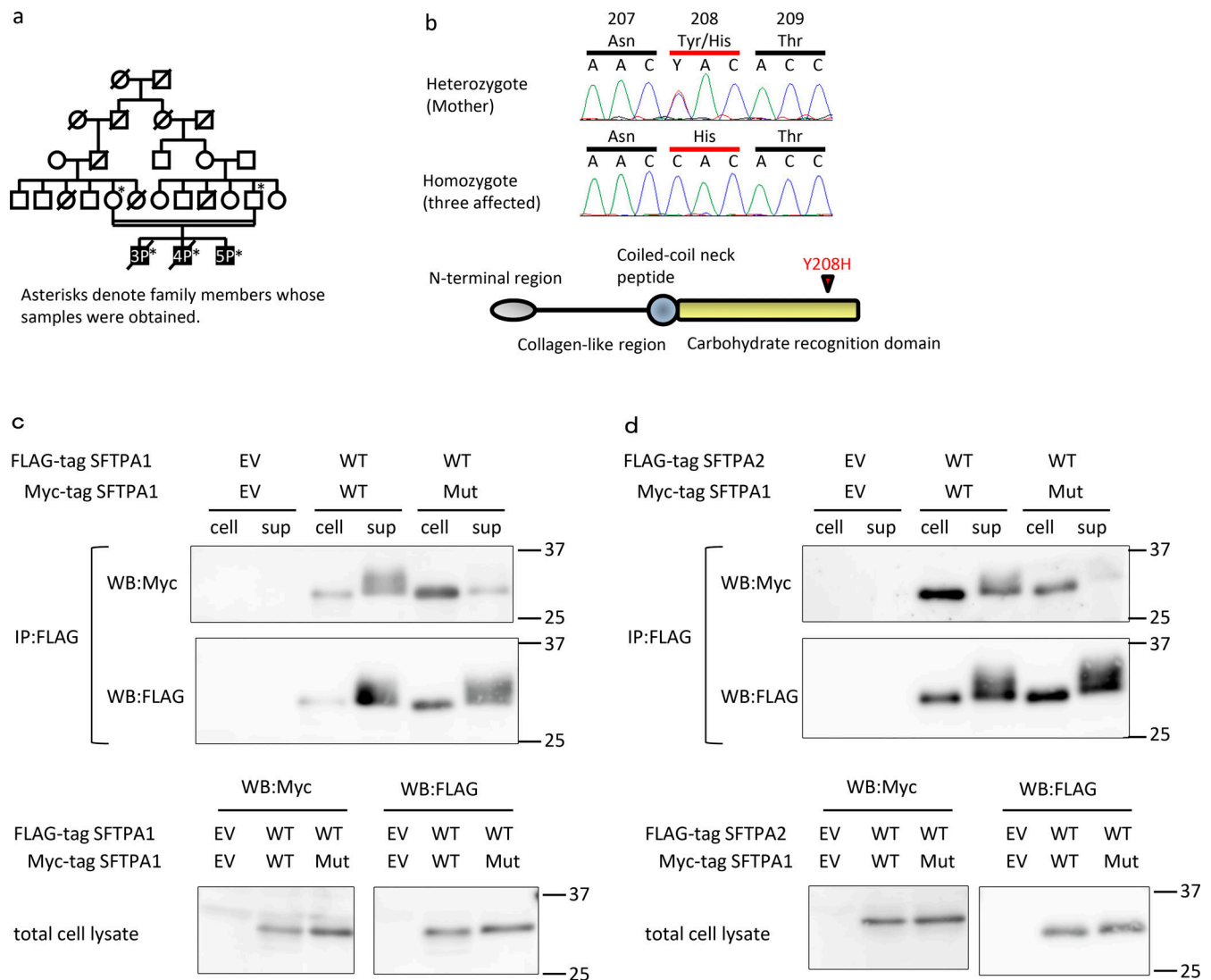


Figure S1. **Identification of an SFTP1 mutation in IPF patients and its effect on the secretion of SFTP1.** (a) Pedigree of a Japanese IPF family: double lines indicate consanguinity, filled black indicates IPF patients, and diagonal lines indicate deceased siblings. P, patient. (b) The heterozygous (parents) or homozygous (patients) missense mutation in *SFTP1* (Y208H) as shown by capillary sequencing. *SFTP1* protein domains: the red arrowhead indicates position of the missense mutation. (c and d) The Flag-tagged *SFTP1* and Myc-tagged *SFTP1* (c; WT or mutant [Mut]) or Flag-tagged *SFTP2* and Myc-tagged *SFTP1* (d; WT or Mut) cDNA was transfected into A549 cells. As a negative control, empty vector (EV) was transfected. 1 d after transfection, the cell pellets (cell) or supernatant (sup) were immunoprecipitated with anti-Flag antibody, and the immunoprecipitates were blotted with an anti-Flag or Myc antibody. As a control, total cell lysates were blotted with the anti-Flag or Myc antibody. WB, Western blot. Data shown are representative of five (c and d) independent experiments.

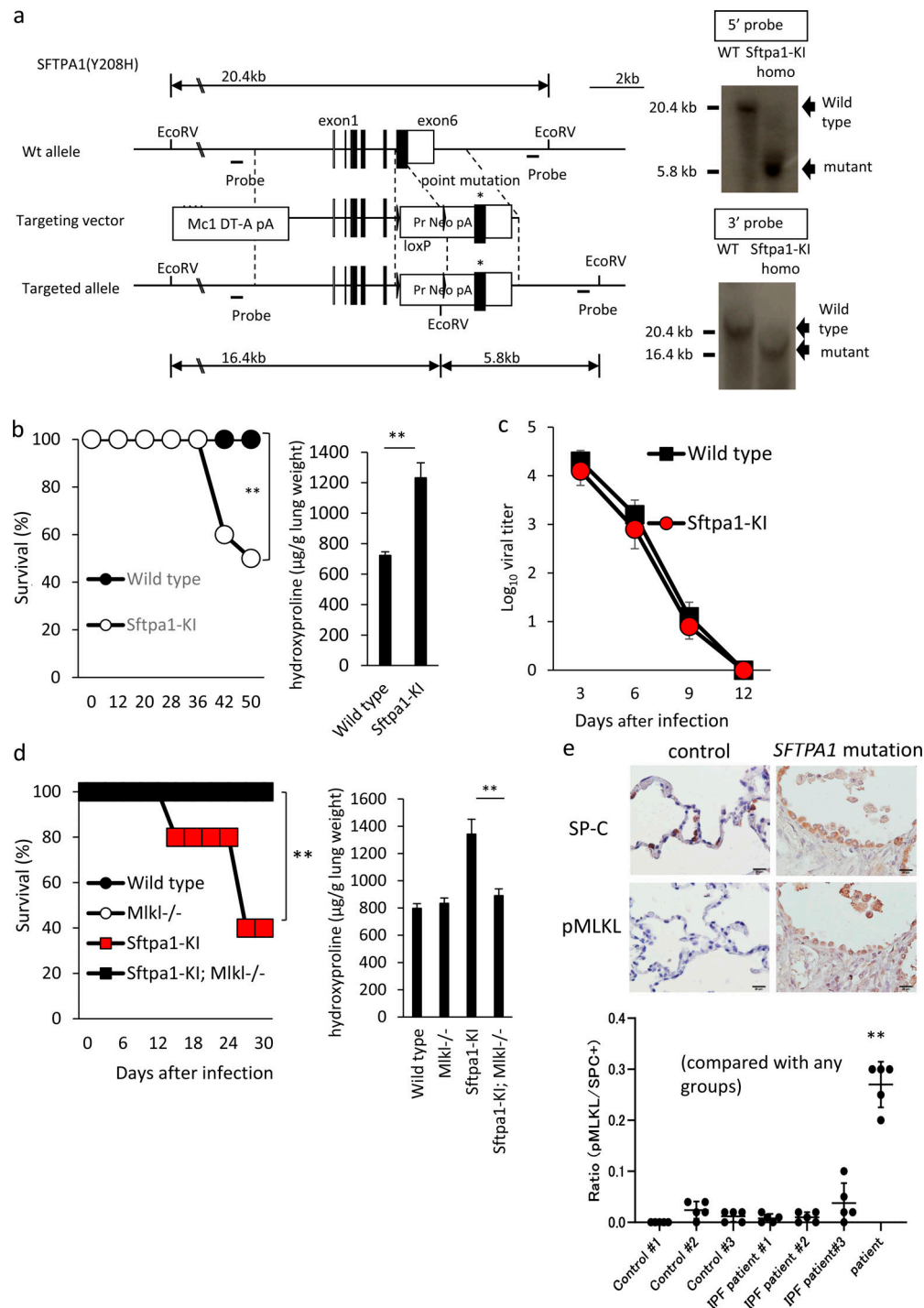


Figure S2. Increased necroptosis in *Sftpa1*-KI mice and IPF patients. (a) The breeding scheme for the construction of *Sftpa1*-KI mice. The point mutation was inserted at position 208 (Y208H). Southern blot analysis of genomic DNA from WT and *Sftpa1*-KI mice. Genomic DNA from mice with homozygous (homo) mutant allele or WT mice was digested with *EcoRI* and blotted with 3' and 5' probes. DT-A, diphtheria toxin fragment A; pA, polyadenylation signal; Pr, promoter. **(b)** Survival analysis of WT (closed circles) or *Sftpa1*-KI mice (open circles; number of mice in each independent experiment is 20). **, $P < 0.01$ by log rank test. Quantification of hydroxyproline contents in WT or *Sftpa1*-KI mice (number of mice in each independent experiment is seven) at the age of 35 wk. Data are means \pm SD. **, $P < 0.01$. **(c)** Virus titer in lung tissue was evaluated in WT (closed square) or *Sftpa1*-KI (red circle) mice infected with IAV. Results are shown as means \pm SD. **(d)** Survival analysis of WT (closed circles), *Mkl1*^{-/-} (open circles), *Sftpa1*-KI (red squares), and *Sftpa1*-KI mice deficient in *Mkl1* (*Sftpa1*-KI; *Mkl1*^{-/-} [closed squares]; number of mice in each independent experiment is 10). **, $P < 0.01$ by log rank test. The data are representative of three independent experiments. Quantification of hydroxyproline contents in WT, *Mkl1*^{-/-}, *Sftpa1*-KI, or *Sftpa1*-KI; *Mkl1*^{-/-} mice (number of mice in each independent experiment is 10) 12 d after IAV infection. Data represent the means \pm SD. **, $P < 0.01$. **(e)** Histological section was stained with anti-SP-C or pMLKL antibody in controls (healthy part of lungs from three lung cancer patients) and three IPF patients without SFTPA1 mutation (#1, #2, and #3) and a patient with SFTPA1 mutation (3P in Fig. S1 a). The scale bar indicates 20 μ m. The ratios of pMLKL-positive cells/SP-C-positive cells in five distinct parts of images are shown. Data are means \pm SD. **, $P < 0.01$. Data shown are representative of five (b–f) independent experiments.

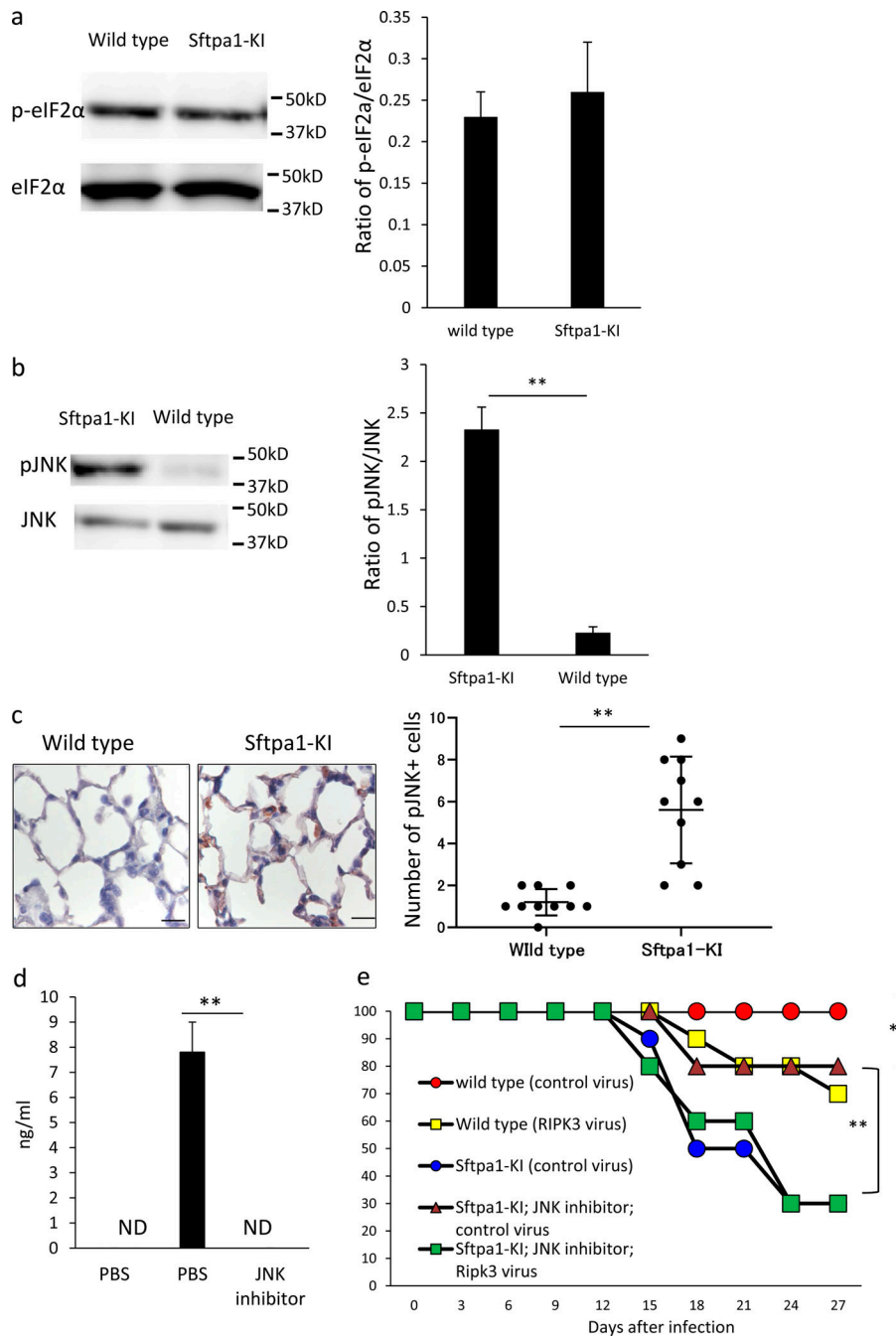


Figure S3. **The inhibition of JNK blocks pulmonary fibrosis.** (a and b) The expression of phosphorylated eIF2 α (a) or phosphorylated JNK (b) in WT or Sftpa1-KI mice at the age of 35 wk was evaluated by Western blotting. Data are means \pm SD. **, $P < 0.01$. (c) The expression of pJNK in WT or Sftpa1-KI mice at the age of 30 wk was evaluated by immunohistochemistry. The pJNK-positive cells (average of the number of pJNK-positive cells in 10 independent fields in right lung) was counted. Data are means \pm SD. **, $P < 0.01$. The scale bar indicates 20 μ m. (d) WT mice were injected with LPS (50 μ g), and serum TNF α was measured 3 h after LPS injection. The JNK inhibitor (30 mg/kg, s.c.) was administered 3 h before LPS injection. Data are means \pm SD. **, $P < 0.01$. The data are representative of two independent experiments. (e) This is an additional set of experiments for Fig. 3 b. Survival of 20-wk-old WT (red circles), WT infected with adenovirus carrying *Ripk3* (yellow squares), Sftpa1-KI mice infected with control virus (blue circles), Sftpa1-KI mice infected with control virus and treated with a JNK inhibitor (brown triangles), or Sftpa1-KI mice infected with *Ripk3*-adenovirus and treated with a JNK inhibitor (green squares; number of mice in each independent experiment is 10). *, $P < 0.05$; **, $P < 0.01$ by log rank test. Data shown are representative of five (a–d) independent experiments.